JACS
JOURNAL OF THE AMERICAN CHEMICAL SOCIETY

Article

pubs.acs.org/JACS

A Protocol to Fabricate Nanostructured New Phase: B31-Type MnS Synthesized under High Pressure

Guanjun Xiao,[†,§] Xinyi Yang,[†,§] Xinxin Zhang,[†] Kai Wang,[†] Xiaoli Huang,[‡] Zhanhui Ding,[‡] Yanming Ma,[†] Guangtian Zou,[†] and Bo Zou*[,†]

[†]State Key Laboratory of Superhard Materials and [‡]College of Physics, Jilin University, Changchun 130012, China

Supporting Information

ABSTRACT: Synthesis of nanomaterials with target crystal structures, especially those new structures that cannot be crystallized in their bulk counterparts, is of considerable interest owing to their strongly structure-dependent properties. Here, we have successfully synthesized and identified new-phase nanocrystals (NCs) associated with orthorhombic MnP-type (B31) MnS by utilizing an effective high-pressure technique. It is particularly worth noting that the generated new structured MnS NCs were captured as expected by quenching the high-pressure phase to the ambient conditions at room temperature. Likewise, the commercially available bulk rocksalt (RS) MnS material underwent unambiguously a reversible phase transition when the pressure was released completely. First-principles calculations further supported that the B31-MnS was more energetically preferable than the RS one under high pressure, which can be plausibly interpreted by the structural buckling with respect to zigzagged arrangements within B31 unit cell. Our findings represent a significant step forward in a deeper understanding of the high-pressure phase diagram of MnS and even provide a promising strategy to prepare desired nanomaterials with new structures that do not exist in their bulk counterparts, thus greatly increasing the choice of materials for a variety of applications.

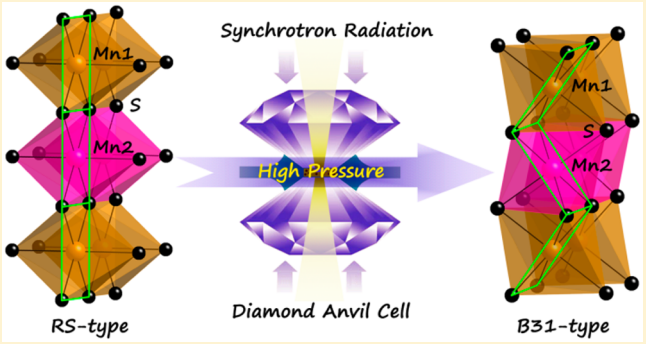

INTRODUCTION

Synthesis of nanomaterials with target crystal structures, especially those new structures which cannot be crystallized in their bulk counterparts, is of considerable interest owing to their strongly structure-dependent properties.[1−3] In this regard, Gupta and co-workers have recently synthesized a newly wurtzite-type $CuIn_xGa_{1-x}S_2$ nanocrystal (NC) by using a solution-based method.[4] Meanwhile, Schaak et al. also reported on a successful preparation of newly structured MnSe NCs via a colloidal synthesis route.[5] All of the aforementioned nanostructures went beyond the presently well-known phases indwelled in the corresponding bulk materials. However, searching for highly desirable alternatives with new nanostructures as well as their effective preparation strategies has still remained exceedingly limited and quite challenging thus far. High-pressure technique has proven to be a powerful tool to develop new materials, especially since the achievement in the 1950s of the diamond anvil cell (DAC).[6−15] In this respect, Zhang et al. has recently impelled sodium chlorides away from the stoichiometric compositions including Na_3Cl and $NaCl_3$, etc., which endowed high pressure a highly attractive route to synthesize novel materials.[16] Meanwhile, Tolbert and Alivisatos, as pioneers, have broken a new ground on high-pressure nanomaterials with respect to structural phase transition of CdSe nanoparticles[17] and initiated the rapid development of high-pressure nanotechnology.[18−27] To date, there have been very few reports by Jiang et al. on the high-pressure nanophases that could as anticipated survive to ambient conditions.[28−30] Nevertheless, the quenchable nanostructured phases as mentioned above were just confined to the existing forms in bulk materials.

Manganese sulfide (MnS) embraces a wide range of electronic and magneto-optical properties on account of the unpaired electrons in high-spin Mn^{2+}, wide band gaps, and distinct magnetic orderings. Under atmospheric pressure, MnS is known to exist in nature as a stable rocksalt (RS) phase and as metastable zinc blende (ZB) and wurtzite (WZ) structures.[31] We have previously investigated the stabilities of metastable ZB- and WZ-MnS NCs under high pressure, which uncovered that both of them would eventually convert into the stable RS phase.[32] The naturally raising question is what if RS-structured MnS was subjected to high pressure? Although intense experimental and theoretical studies have contributed to the pressure-induced phase transitions in RS-MnS, their results offered limited understanding of transition process and remained elusive. In this respect, Clendenen and co-workers observed a tetragonal distortion without an exact structure at roughly 10 GPa.[33] Aiming at the structure determinations, Kraft and Greuling detected a structural phase transition from the RS

Received: June 4, 2015
Published: August 5, 2015

DOI: 10.1021/jacs.5b05629
J. Am. Chem. Soc. 2015, 137, 10297−10303

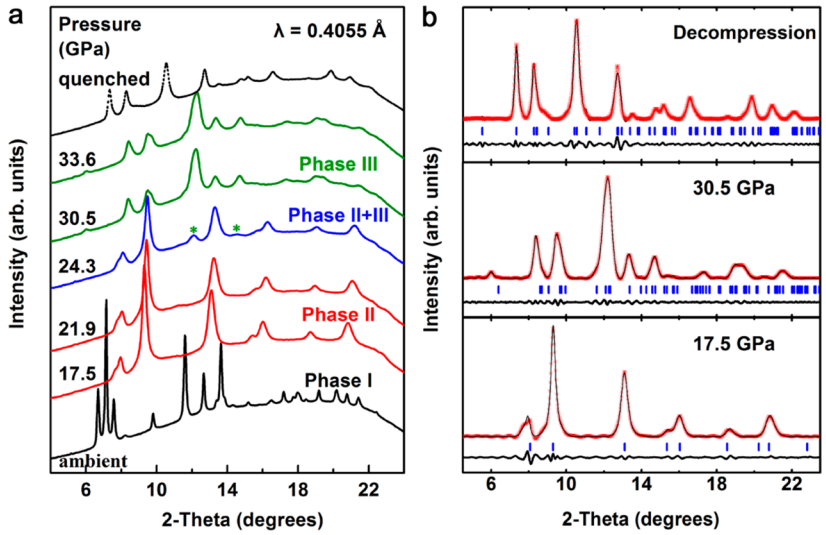

Figure 1. (a) Representative *in situ* ADXRD patterns of WZ-MnS nanorods with the presence of silicon oil as PTM during the high-pressure experiments. (b) Rietveld refinements of the experimental (red fork), simulated (black profile), and difference (black line) ADXRD patterns of phase II at 17.5 GPa, phase III at the pressure of 30.5 GPa, and quenched phase upon completely releasing the pressure to ambient conditions. Therein, blue vertical markers indicate the corresponding Bragg reflections.

type (B1) to the GeS type (B16) at 7.2 GPa,[34] whereas, a conflicting report by McCammon et al. showed no evidence of either phase transition occurring even up to the pressure of approximately 21 GPa.[35] Until 1993, Sweeney and Heinz further demonstrated a phase transition of RS-MnS at 26 GPa from B1 phase to an undefined high-pressure one with symmetry lower than hexagonal.[36] Therefore, the identification and retention of the long-puzzling high-pressure phase of MnS have been of great concern to date.

To this end, we here devoted ourselves to investigating the high-pressure behaviors of RS-MnS, primarily focusing on the nanocrystalline forms. We have succeeded in identifying a new high-pressure nanophase associated with orthorhombic MnP-type (B31) MnS by utilizing an effective *in situ* angle dispersive synchrotron X-ray diffraction technique. It is particularly worth noting that the generated new structured MnS NCs were quenchable as expected to the ambient conditions at room temperature, which allows access to further exploring the potentially unusual properties. This work represents a significant step forward in deeply understanding the high-pressure phase diagram of MnS. Likewise, the commercially available bulk RS-MnS material underwent unambiguously a reversible phase transition when the pressure was released completely. First-principles calculations further supported that the B31-type MnS was more energetically preferable under high pressure, induced significantly by the structural buckling toward zigzagged arrangements within its unit cell. This work offers a potential pathway for exploiting highly desired nanomaterials with new structures that do not exist in their bulk counterparts, thus largely extending the current physical world for the practical applications.

EXPERIMENTAL SECTION

Characterization. Transmission electron microscopy (TEM) and high-resolution TEM images were performed on a JEM-2200FS with an emission gun operating at 200 kV. The field-emission scanning electron microscopy (FESEM) measurements were carried out with a Magellan-400 (FEI Company). Energy-dispersive X-ray spectroscopy (EDX) was collected from the attachment to the Magellan-400. Fourier transform infrared (FTIR) spectra were recorded with a PerkinElmer spectrometer (Spectrum One B). The sample was pressed into a tablet with dried potassium bromide (KBr). Magnetic property measurements were conducted on a Quantum Design MPMS superconducting quantum interference device (SQUID) VSM magnetometer. The WZ-MnS nanorods and RS-MnS nanocubes were synthesized through the standard airless techniques as described elsewhere.[32,37] Both of them were utilized as pressurized samples in our high-pressure experiments which were conducted in a symmetric DAC furnished with a pair of 400 μm culet diamonds at room temperature. The prepared nanostructured MnS NCs were enclosed into a ~100 μm-diameter hole of the T301 stainless-steel compressible gasket. Silicon oil was utilized as the pressure transmitting medium (PTM) which was purchased from the Dow Corning Corporation (Midland, MI). Pressure determination was achieved by the fluorescence spectrum of the ruby.[38] *In situ* angle dispersive synchrotron X-ray diffraction (ADXRD) patterns of MnS nanorods under high pressure were recorded at HPCAT's 16 BMD beamline facility of the Advanced Photon Source (APS) at Argonne National Laboratory (ANL), U.S.A., with a wavelength of 0.4055 Å. The ADXRD measurements of MnS nanocubes were conducted on the X17C beamline of Brookhaven National Laboratory (BNL), U.S.A., with a wavelength of 0.4064 Å. And the ADXRD patterns of bulk MnS material were collected at beamline 15U1, Shanghai Synchrotron Radiation Facility (SSRF), and 4W2 beamline of Beijing Synchrotron Radiation Facility (BSRF), China. Both of the beamline stations at SSRF and BSRF exploited a wavelength of 0.6199 Å. The Bragg diffraction rings were collected and integrated on the basis of FIT2D program, yielding one-dimensional intensity versus diffraction angle 2θ patterns.[39] *In situ* high-pressure UV−vis−NIR absorption spectra were collected by an optical fiber spectrometer (Ocean Optics, QE65000) at room temperature. The samples were placed into a ~120 μm-diameter hole that was drilled on a pre-indented 40 μm-thickness T301 stainless-steel gasket. Silicon oil was also used as the PTM to keep in step with high-pressure ADXRD measurements. To guarantee the quantity of samples for magnetic performance, high-pressure experiments on RS-MnS nanocubes were carried out in a Walker module multianvil apparatus (Rockland Ltd., U.S.A.), subsequently by collecting the quenched products for further magnetic characterization. Therein, the pressure was given by a calibration curve that was established by determining the applied loads corresponding to the phase transformation pressures of bismuth, thallium, and barium.

Computation. First-principles calculations were performed using the local density functional approximation (LDA) method as implemented in the Vienna *ab initio* simulation package (VASP)

DOI: 10.1021/jacs.5b05629
J. Am. Chem. Soc. 2015, 137, 10297−10303

Table 1. Experimental Lattice Parameters and Atomic Positions within Its Unit Cell for the Recovered Orthorhombic B31-Type MnS Nanorods, Derived from the Rietveld Refinements in Figure 1

					atomic coordinates (fractional)		
phase	space group	Z	lattice parameters (Å, °)	atom	x	y	z
B31-MnS	*Pnma*	4	a = 5.5807(1)	Mn (4c)	0.9311(3)	0.2500(0)	0.0648(4)
			b = 3.6309(3)	S (4c)	0.9554(6)	0.2500(0)	0.5683(9)
			c = 6.2799(5)				
			$\alpha = \beta = \gamma = 90$				

code.[40] To give a correct description of the strong on-site Coulomb correlations among the localized Mn-d electrons, we had to take into account the coulomb U and exchange energy J during the calculations, in which the values of U and J were set to be 6.0 and 0.87 eV, respectively. Furthermore, the Monkhorst−Pack (MP) grids with 4 × 4 × 4 and 6 × 6 × 10 accompanied by an energy cutoff of 500 eV were employed for the RS-phase and B31-type MnS.

RESULTS AND DISCUSSION

***In Situ* High-Pressure Experiments.** As shown in Figure 1a, *in situ* ADXRD patterns at selected pressures of the WZ-MnS nanorods were performed at room temperature with an incident monochromatic wavelength of 0.4055 Å. It turns out that when the pressure increased to about 17.5 GPa, the original WZ-type MnS (phase I) nanorods with 4-fold coordination transformed into 6-fold coordinated RS-structure MnS NCs, which is in good accordance with our previous report.[32] All the diffraction peaks of the obtained RS phase simultaneously shifted to higher angles with increasing pressure, which corroborated the volume compression. With further pressurizing the obtained RS-type MnS NCs to 24.3 GPa, two distinct new peaks located in 2θ range of 13−15° appeared, indicating the formation of another new phase. The new phase remained stable to ∼33.6 GPa and could not be assigned to any previously known phases in bulk MnS material. Particularly note that the generated new phase can be retained even when completely releasing the pressure to ambient conditions. This manifests that new structured MnS NCs could be accessed successfully by applying the effective high-pressure technique through an irreversible structural phase transition. Rietveld refinements of phase II at 17.5 GPa and phase III at the pressure of 30.5 GPa are well fitted and can be indexed to the RS-type and B31 structure, respectively (Figure 1b). Furthermore, the well-fitted refinements of the quenched ADXRD pattern indeed confirmed the recovered new phase being orthorhombic B31-type MnS polymorph with the space group of D_{2h}^{16}-*Pnma* (a = 5.5807(1) Å, b = 3.6309(3) Å, and c = 6.2799(5) Å, as can be seen in Table 1). The retention of high-pressure phase should be ascribed to the significant hysteresis of phase transformation for NCs in the process of decompression as compared to their bulk counterparts. This involved sluggishness was largely dictated by the unsaturated coordination of surface atoms and thus enhanced surface energy in nanomaterials.[41,42] Furthermore, the recovered samples of nanorods are largely deformed and aggregated, which are mainly attributed to the deviatoric stress induced by the nonhydrostatic pressure at above 10 GPa. Thereby, in addition to the nanosize and shape effect, aggregation-resulted internanorod structures should be another crucial factor for the preservation of B31 phase at atmospheric conditions. In a word, high pressure enables us to efficiently capture the new phase of alabandite NCs, that is orthorhombic B31-type MnS.

Lattice constants versus increasing pressures exhibit declining trend for both RS- and B31-type MnS NCs (Figure 2).

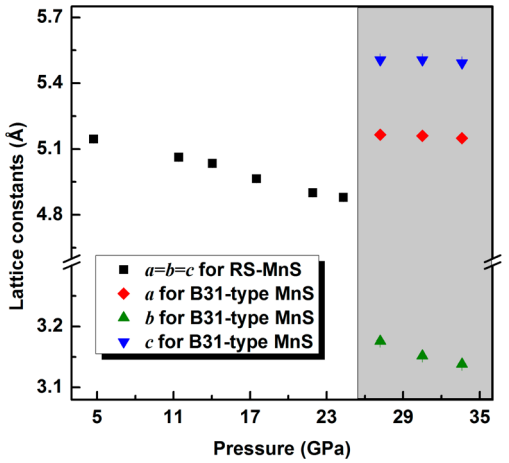

Figure 2. Lattice constants (a, b, and c) of RS-MnS NCs and B31-type MnS NCs as a function of the increasing pressures up to 33.6 GPa. Detailed definitions of various symbols are interpreted in the figure.

Moreover, it also demonstrates that the b-axis direction of B31-type MnS was more sensitive to the applied external pressure with a significant compression rate. The experimental $P-V$ data ranging from ambience to 33.6 GPa were fitted by means of the well-established Birch−Murnaghan equation of state[43] (Figure 3). Intriguingly, the isothermal bulk modulus B_0 for B31 phase MnS NCs was estimated to be about 380.1(1) GPa with B_0' fixed as 4, which was much larger than that of original RS-MnS

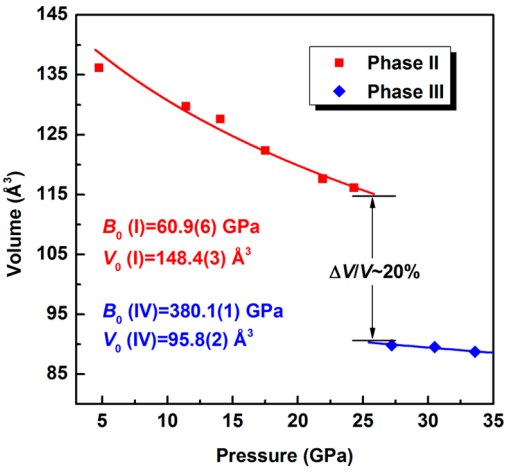

Figure 3. Experimental volumes versus applied pressures ranging from ambience to 33.6 GPa for the phases II and III of MnS NCs. The dashed lines represent the third-order fitted Birch−Murnaghan EOS functions to the measured $P-V$ data.

DOI: 10.1021/jacs.5b05629
J. Am. Chem. Soc. 2015, 137, 10297−10303

NCs (60.9(6) GPa), indicating the highly difficult compressibility toward B31-type MnS NCs. The enhancement of the bulk modulus may be attributed to the surface effect or structure disorder. In addition, the remarkable volume drop by ∼20% from RS-phase to B31-structure MnS evidenced the first-order phase transition.

We further examined the phase transition evolution of original MnS NCs by performing *in situ* high-pressure optical characterization. Figure 4 represents the typical profile of band

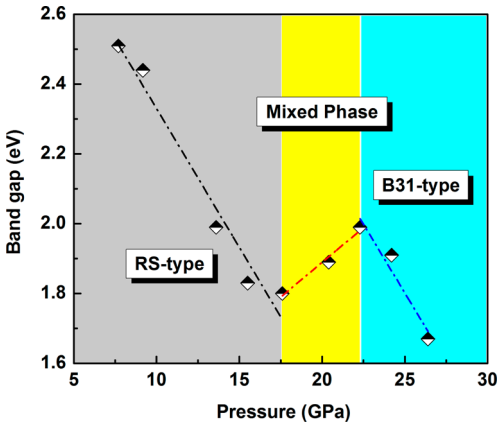

Figure 4. Typical profile of band gaps against pressures for WZ-MnS nanorods measured *in situ* in a DAC apparatus. Therein, dashed lines represent the corresponding linear fitting toward different regions.

gaps as a function of pressures for MnS NCs measured in a DAC apparatus. We can observe that band gaps of RS-MnS NCs decrease linearly with increasing pressure. However, when the pressure reached roughly 17.6 GPa, band gap of the compressed samples suddenly ascended. This stark change indicates the onset of phase transition evolving from RS-MnS to B31-structure MnS. The RS-phase MnS indwelled in mixed phases gradually vanished when the pressure approached to the critical point of about 22.3 GPa. At the moment, we proposed that the phase transformation to B31-type MnS was completely achieved. Subsequently, the band gaps dropped abruptly with further elevating pressure to 26.4 GPa.

As shown in Figure 5a, TEM image of the decompressed sample indicates that the shape of MnS nanorods could be maintained after the high-pressure treatment by contrast to its original pressurized morphology (Figure S1). Moreover, the interplanar spacing collected on an individual nanorod was measured to be about 0.19 nm, which corresponds to the (211) facet of the orthorhombic B31 phase MnS (Figure 5b). The corresponding fast Fourier transform (FFT) pattern strongly validates the single-crystalline nature (top inset in Figure 5b). We also investigated the band gap E_g on the captured B31-type MnS NCs in terms of Kubelka–Munk transformations:[44]

$$(\alpha h\nu)^2 = A(h\nu - E_g) \quad (1)$$

where A and $h\nu$ are the edge-width parameter and the incident photon energy, respectively. As a consequence, the optical band gap E_g of B31-type MnS NCs was estimated to be ca. 2.7 eV determined with the x-axis intercept by extrapolating the linear portion of the $(\alpha h\nu)^2$ versus $h\nu$ plot to $\alpha = 0$ (Figure 5c). Furthermore, we calculated the electronic band structure of B31-phase MnS at the temperature of 0 K and atmospheric pressure, as shown in Figure 5d. The results suggest that the B31-type MnS exhibits a semiconductor characteristic with an

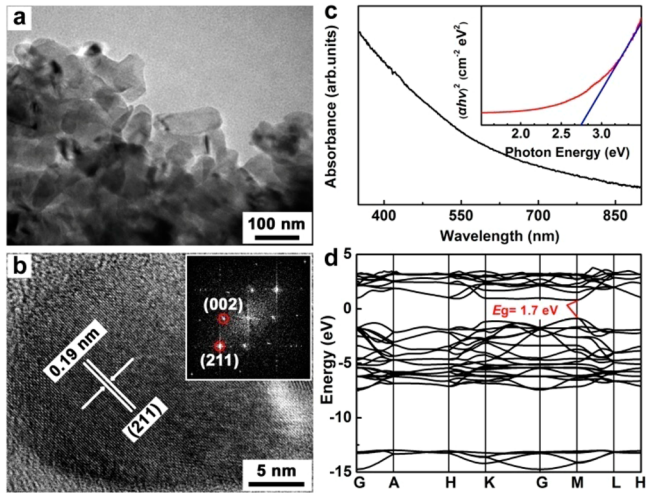

Figure 5. (a) TEM image of decompressed B31-type MnS nanorods. (b) HRTEM image of the obtained B31-type MnS nanorods when the pressure was completely released to ambient conditions. Inset shows the corresponding FFT pattern. (c) UV–vis–NIR absorption spectrum of the synthesized B31-type MnS nanorods. Inset depicts the plot of $(\alpha h\nu)^2$ versus $h\nu$ according to Kubelka–Munk transformations. (d) Calculated electronic band structure of B31-type MnS at the temperature of 0 K and ambient pressure.

energy gap of about 1.7 eV. The quantum confinement effect along with the underestimation of theoretical computations in band gap should rationally account for this stark discrepancy between the experimental and theoretical results, even if the diameter of nanorods is much larger than the bulk exciton Bohr radius.[45−47]

This intriguing discovery strongly triggered us to explore whether the morphology of originally compressed samples would affect the aforementioned experimental results. Typically, cube-like RS-MnS NCs were held between the opposed diamond anvils at room temperature. We conducted *in situ* high-pressure ADXRD measurements toward RS-MnS nanocubes by utilizing silicon oil as the PTM (Figure S2a). It turns out that the RS structure of MnS nanocubes remained stable up to 11.6 GPa, where an additional peak appeared, indicating the occurrence of the phase transition. With the increasing pressure, the new yielded phase kept stable up to the maximum pressure of 31.7 GPa in present study. Likewise, the well-fitted Rietveld refinements of selected ADXRD patterns at 0.9 and 23.0 GPa further verified that the initial structure and the obtained new phase adopted RS- and B31-type MnS, respectively (Figure S2b). Similarly, the B31-type MnS NCs could also be conserved after being released to atmospheric pressure, validating the feasibility of our high-pressure approach to fabricate newly structured nanomaterials (Figure S3). Moreover, the decompressed samples still retained its initial good crystallinity and cube-like morphology (Figures S4 and S5). The band gap of quenched products was found to be 3.1 eV which was determined by the extrapolation of the absorption spectrum in the band edge region (Figure S6). The much smaller size of nanocubes in comparison with B31-nanorods made a dominant contribution to the larger band gap. In fact, the resulting samples were passivated by the organic ligand of oleylamine (OLA), which often acts as a surfactant in NCs synthesis as reported elsewhere.[48] This was further confirmed by the FTIR spectra recorded with a PerkinElmer spectrometer (Spectrum One B), as shown in Figure S7. The

DOI: 10.1021/jacs.5b05629
J. Am. Chem. Soc. 2015, 137, 10297−10303

FTIR spectra of WZ-MnS nanorods and RS-MnS nanocubes could be well assigned to the vibrational mode of the OLA molecule. In a word, both WZ-MnS nanorods and RS-MnS nanocubes are passivated by the organic ligand of OLA on the surface after the washing treatment. Moreover, high pressure is capable of tuning changes of the chain structures and consequent lengths of the coordinated OLA. An OLA molecule, $CH_3(CH_2)_7CH{=}CH(CH_2)_8NH_2$ has a chain length of ~2.05 nm, but it is mostly buckled with a certain angle (Scheme S1). Upon being submitted to pressure, the buckled OLA chains would open up to straighten.[49] Furthermore, the surface-bonded OLA ligands indeed act as a shear stress absorber to greatly enhance elastic strength of samples, thus encouraging ones to develop strong building blocks with improved elastic strength. Considering the experimentally realizable phase transition pressure of B31-MnS nanocubes in Walker-type multianvil apparatus, we further investigated the magnetic response of the quenched B31-MnS nanocubes, which exhibited a paramagnetism at 5 K (Figure S8).

Furthermore, we performed the *in situ* high-pressure experiments on the commercially available bulk RS-MnS material which was purchased from Alfa Aesar. As shown in Figure 6, *in situ* ADXRD patterns at selected pressures of bulk

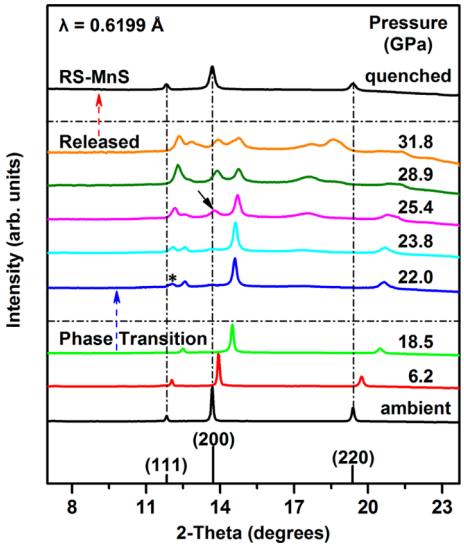

Figure 6. Typical *in situ* ADXRD patterns of the commercially available bulk RS-MnS with a wavelength of 0.6199 Å under high pressure. The symbols of asterisk and arrow correspond to the new phase, orthorhombic B31-type MnS.

RS-MnS were collected with a wavelength of 0.6199 Å. The RS structure extended up to the pressure of 18.5 GPa. Subsequently, an extra new Bragg peak denoted by an asterisk emerged as soon as the loading pressure reached 22.0 GPa, signifying the onset of initial structural phase transition. The peak marked with an arrow also corresponded to the generated new phase. Rietveld refinements of the ADXRD pattern at 31.8 GPa confirmed that the observed new phase represented a characteristic feature of orthorhombic B31 structure (Figure S9). Nevertheless, the decompressed ADXRD pattern retrieved its original RS structure again when the pressure was released completely, indicating a reversible phase transition as deduced from the quenched profile in Figure 6. Accordingly, our results strongly suggest that the application of high pressure could open a robust route to fabricate nanomaterials with new structures that failed to be quenchable for the corresponding bulk counterparts.

We further calculated the energy differences between the RS- and B31-phase MnS covering the range up to 40 GPa, as shown in Figure 7. Enthalpy here was the Gibbs free energy as the

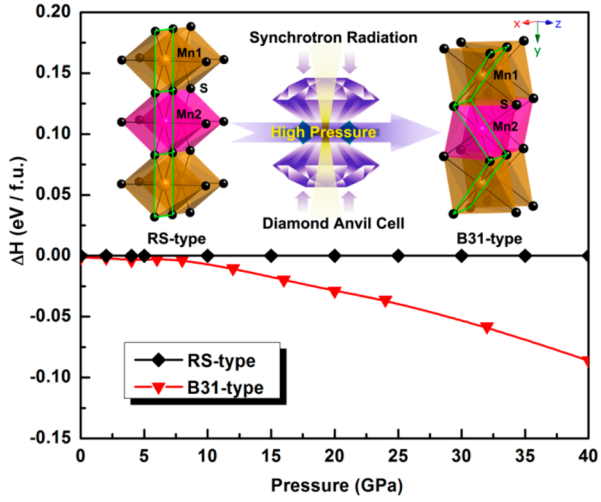

Figure 7. Pressure dependence of calculated enthalpy differences per formula unit for orthorhombic B31-type MnS relative to cubic RS-type MnS. Inset on the top panel shows the schematic illustration with respect to polyhedral views crystal structures of RS- and B31-type MnS under high pressure.

calculations were carried out at the temperature of 0 K. It is unmistakable that the energy of B31-type structure was very close to that of RS phase below 8 GPa. Since the driving force of a structural transformation is the reduction in Gibbs free energy, the apparent decrease in the enthalpy of the B31 phase after roughly 10 GPa indicates that B31-type MnS was more energetically preferable under high pressure. In contrast to bulk MnS material, the unique nanostructures of MnS NCs and the inevitable thermodynamic influence should be responsible for the retention of high-pressure new phase by aggravating the fluctuation of the subtle enthalpy differences under atmospheric pressure. Moreover, so as to further elucidate the transformation process at a glance, the inset on the top panel of Figure 7 depicts the schematic illustrations of crystal structures for RS- and B31-type MnS under high pressure. Viewed from the polyhedral structures concerning both two phases, one Mn atom and six neighboring S atoms integrally formed a MnS_6 octahedron. Noticeably, the adjacent MnS_6 octahedrons in B31 phase mutually shared the same surface rather than being connected by the edge perpendicular to the interlayers for RS-type MnS. It is evidenced that the MnS_6 octahedron in B31 phase arranged much more compacted than that in RS phase, which was greatly improved by the creation of zigzagged MnS_4 planes inside the MnS_6 octahedron along the *b*-axis direction. The rearrangements in the structural buckling may profoundly facilitate the phase transformation to accommodate the increased external pressure. Furthermore, the unambiguous pressure response in the *b*-axis direction deduced from the profile of Figure 2 further supports the feasible phase transition routines.

DOI: 10.1021/jacs.5b05629
J. Am. Chem. Soc. 2015, 137, 10297−10303

CONCLUSIONS

In summary, we have synthesized and identified new phase NCs associated with orthorhombic B31-type MnS by utilizing an effective high-pressure technique. This achievement unravels the long-lasting puzzle about the high-pressure structures of RS-MnS. Particularly, the generated new structured B31-MnS NCs were recoverable as expected to the ambient conditions at room temperature. The morphology of decompressed samples could be maintained after the high-pressure treatment despite their original pressurized shape. Nevertheless, the decompressed ADXRD pattern of the commercially available bulk RS-MnS material retrieved its original RS structure again when the pressure was released completely, indicating a reversible phase transition. First-principles calculations further supported that the B31-type MnS was more energetically preferable under high pressure, driven by the structural buckling with respect to zigzagged arrangements that are highly favorable for the phase transformation into the resulting B31 phase. In contrast to bulk MnS material, the unique nanostructures of MnS NCs and the inevitable thermodynamic influence should be responsible for the retention of high-pressure new phase by aggravating the fluctuation of subtle enthalpy differences under atmospheric pressure. Our findings offer an attractive route for harvesting long-sought MnS nanomaterials with new structures that do not exist in their bulk counterparts.

ASSOCIATED CONTENT

Supporting Information

The Supporting Information is available free of charge on the ACS Publications website at DOI: 10.1021/jacs.5b05629.

Additional experimental section, lattice parameters for B31-type MnS, *P*−*V* profiles, TEM/HRTEM/FESEM images, FTIR spectra, ADXRD patterns under high pressure and Rietveld refinements profiles for RS-MnS nanocubes and bulk RS-MnS (PDF)

AUTHOR INFORMATION

Corresponding Author

*zoubo@jlu.edu.cn

Author Contributions

§These authors contributed equally.

Notes

The authors declare no competing financial interest.

ACKNOWLEDGMENTS

Many thanks to Mr Bo Zhou and Mr Yuancun Qiao for the help in partial experiments. We gratefully acknowledge funding support from the National Natural Science Foundation of China (nos. 91227202, 11404135, and 11204101), Changbai Mountain Scholars Program (no. 2013007), RFDP (no. 20120061130006), the National Basic Research Program of China (no. 2011CB808200), the China Postdoctoral Science Foundation (nos. 2014M550171 and 2014M561281), and Jilin Provincial Science & Technology Development Program (no. 20150520087JH). This work was performed at HPCAT (Sector 16), Advanced Photon Source (APS), Argonne National Laboratory (ANL), X17C-Brookhaven National Laboratory (BNL), beamline 15U1, Shanghai Synchrotron Radiation Facility (SSRF), and 4W2 HP-Station, Beijing Synchrotron Radiation Facility (BSRF) which is supported by Chinese Academy of Sciences (grant nos. KJCX2-SW-N20 and KJCX2-SW-N03). Therein, HPCAT is supported by CIW, CDAC, UNLV, and LLNL through funding from DOENNSA, DOE-BES, and NSF. APS is supported by DOE-BES, under contract no. DE-AC02-06CH11357.

REFERENCES

(1) Park, K. H.; Jang, K.; Kim, S.; Kim, H. J.; Son, S. U. *J. Am. Chem. Soc.* **2006**, *128*, 14780−14781.
(2) Ji, T.; Jian, W.; Fang, J. *J. Am. Chem. Soc.* **2003**, *125*, 8448−8449.
(3) Xiao, N.; Zhu, L.; Wang, K.; Dai, Q.; Wang, Y.; Li, S.; Sui, Y.; Ma, Y.; Liu, J.; Liu, B.; Zou, G.; Zou, B. *Nanoscale* **2012**, *4*, 7443−7447.
(4) Wang, Y.; Zhang, X.; Bao, N.; Lin, B.; Gupta, A. *J. Am. Chem. Soc.* **2011**, *133*, 11072−11075.
(5) Sines, I. T.; Misra, R.; Schiffer, P.; Schaak, R. E. *Angew. Chem., Int. Ed.* **2010**, *49*, 4638−4640.
(6) Ma, Y.; Eremets, M.; Oganov, A. R.; Xie, Y.; Trojan, I.; Medvedev, S.; Lyakhov, A. O.; Valle, M.; Prakapenka, V. *Nature* **2009**, *458*, 182−185.
(7) Zhu, L.; Liu, H.; Pickard, C. J.; Zou, G.; Ma, Y. *Nat. Chem.* **2014**, *6*, 644−648.
(8) McMillan, P. F. *Nat. Mater.* **2002**, *1*, 19−25.
(9) Inaguma, Y.; Yoshida, M.; Katsumata, T. *J. Am. Chem. Soc.* **2008**, *130*, 6704−6705.
(10) Inaguma, Y.; Aimi, A.; Shirako, Y.; Sakurai, D.; Mori, D.; Kojitani, H.; Akaogi, M.; Nakayama, M. *J. Am. Chem. Soc.* **2014**, *136*, 2748−2756.
(11) Ovsyannikov, S. V.; Abakumov, A. M.; Tsirlin, A. A.; Schnelle, W.; Egoavil, R.; Verbeeck, J.; Van Tendeloo, G.; Glazyrin, K. V.; Hanfland, M.; Dubrovinsky, L. *Angew. Chem., Int. Ed.* **2013**, *52*, 1494−1498.
(12) Song, Y.; Manaa, M. R. *J. Phys. Chem. C* **2012**, *116*, 2059−2060.
(13) Xiao, G.; Zhu, C.; Ma, Y.; Liu, B.; Zou, G.; Zou, B. *Angew. Chem., Int. Ed.* **2014**, *53*, 729−733.
(14) Xiao, G.; Wang, K.; Zhu, L.; Tan, X.; Qiao, Y.; Yang, K.; Ma, Y.; Liu, B.; Zheng, W.; Zou, B. *J. Phys. Chem. C* **2015**, *119*, 3843−3848.
(15) Cheng, J. G.; Matsubayashi, K.; Wu, W.; Sun, J. P.; Lin, F. K.; Luo, J. L.; Uwatoko, Y. *Phys. Rev. Lett.* **2015**, *114*, 117001.
(16) Zhang, W.; Oganov, A. R.; Goncharov, A. F.; Zhu, Q.; Boulfelfel, S. E.; Lyakhov, A. O.; Stavrou, E.; Somayazulu, M.; Prakapenka, V. B.; Konôpková, Z. *Science* **2013**, *342*, 1502−1505.
(17) Tolbert, S. H.; Alivisatos, A. P. *Science* **1994**, *265*, 373−376.
(18) Wang, Z.; Schliehe, C.; Wang, T.; Nagaoka, Y.; Cao, Y. C.; Bassett, W. A.; Wu, H.; Fan, H.; Weller, H. *J. Am. Chem. Soc.* **2011**, *133*, 14484−14487.
(19) Li, B.; Wen, X.; Li, R.; Wang, Z.; Clem, P. G.; Fan, H. *Nat. Commun.* **2014**, *5*, 4179.
(20) Wu, H.; Wang, Z.; Fan, H. *J. Am. Chem. Soc.* **2014**, *136*, 7634−7636.
(21) Wu, H.; Bai, F.; Sun, Z.; Haddad, R. E.; Boye, D. M.; Wang, Z.; Huang, J. Y.; Fan, H. *J. Am. Chem. Soc.* **2010**, *132*, 12826−12828.
(22) Wu, H.; Bai, F.; Sun, Z.; Haddad, R. E.; Boye, D. M.; Wang, Z.; Fan, H. *Angew. Chem., Int. Ed.* **2010**, *49*, 8431−8434.
(23) San-Miguel, A. *Chem. Soc. Rev.* **2006**, *35*, 876−889.
(24) Gurlo, A. *Angew. Chem., Int. Ed.* **2010**, *49*, 5610−5612.
(25) Bian, K.; Wang, Z.; Hanrath, T. *J. Am. Chem. Soc.* **2012**, *134*, 10787−10790.
(26) Lü, X.; Hu, Q.; Yang, W.; Bai, L.; Sheng, H.; Wang, L.; Huang, F.; Wen, J.; Miller, D. J.; Zhao, Y. *J. Am. Chem. Soc.* **2013**, *135*, 13947−13953.
(27) Podsiadlo, P.; Lee, B.; Prakapenka, V. B.; Krylova, G. V.; Schaller, R. D.; Demortière, A.; Shevchenko, E. V. *Nano Lett.* **2011**, *11*, 579−588.
(28) Wang, H.; He, Y.; Chen, W.; Zeng, Y. W.; Stahl, K.; Kikegawa, T.; Jiang, J. Z. *J. Appl. Phys.* **2010**, *107*, 033520.
(29) Zhang, C.; Dai, R.; Sui, Z.; Chen, Q.; Wang, Z.; Yuan, X.; Zhang, Z.; Ding, Z. *Chem. Phys. Lett.* **2014**, *612*, 138−142.

DOI: 10.1021/jacs.5b05629
J. Am. Chem. Soc. 2015, 137, 10297−10303

(30) Saha, S.; Gadagkar, V.; Maiti, P. K.; Muthu, D. V. S.; Golberg, D.; Tang, C.; Zhi, C.; Bando, Y.; Sood, A. K. *J. Nanosci. Nanotechnol.* **2007**, *7*, 1810−1814.
(31) Qi, K.; Selvaraj, R.; Jeong, U.; AlKindy, S. M. Z.; Sillanpaa, M.; Kim, Y.; Tai, C. *RSC Adv.* **2015**, *5*, 9618−9620.
(32) Yang, X.; Wang, Y.; Wang, K.; Sui, Y.; Zhang, M.; Li, B.; Ma, Y.; Liu, B.; Zou, G.; Zou, B. *J. Phys. Chem. C* **2012**, *116*, 3292−3297.
(33) Clendenen, R. L.; Drickamer, H. G. *J. Chem. Phys.* **1966**, *44*, 4223−4228.
(34) Kraft, A.; Greuling, B. *Cryst. Res. Technol.* **1988**, *23*, 605−608.
(35) McCammon, C. *Phys. Chem. Miner.* **1991**, *17*, 636−641.
(36) Sweeney, J. S.; Heinz, D. L. *Phys. Chem. Miner.* **1993**, *20*, 63−68.
(37) Yang, X.; Wang, Y.; Sui, Y.; Huang, X.; Cui, T.; Wang, C.; Liu, B.; Zou, G.; Zou, B. *Langmuir* **2012**, *28*, 17811−17816.
(38) Mao, H.; Xu, J.-A.; Bell, P. *J. Geophys. Res.* **1986**, *91*, 4673−4676.
(39) Hammersley, A.; Svensson, S.; Hanfland, M.; Fitch, A.; Hausermann, D. *High Pressure Res.* **1996**, *14*, 235−248.
(40) Kresse, G.; Joubert, D. *Phys. Rev. B: Condens. Matter Mater. Phys.* **1999**, *59*, 1758−1775.
(41) McHale, J. M.; Auroux, A.; Perrotta, A. J.; Navrotsky, A. *Science* **1997**, *277*, 788−791.
(42) Baranov, A. N.; Sokolov, P. S.; Tafeenko, V. A.; Lathe, C.; Zubavichus, Y. V.; Veligzhanin, A. A.; Chukichev, M. V.; Solozhenko, V. L. *Chem. Mater.* **2013**, *25*, 1775−1782.
(43) Birch, F. *J. Geophys. Res.* **1978**, *83*, 1257−1268.
(44) Hagfeldt, A.; Graetzel, M. *Chem. Rev.* **1995**, *95*, 49−68.
(45) Yu, H.; Li, J.; Loomis, R. A.; Gibbons, P. C.; Wang; Buhro, W. E. *J. Am. Chem. Soc.* **2003**, *125*, 16168−16169.
(46) Li, D.; Zhang, J.; Xiong, Q. *ACS Nano* **2012**, *6*, 5283−5290.
(47) Perdew, J. P. *Int. J. Quantum Chem.* **1985**, *28*, 497−523.
(48) Mourdikoudis, S.; Liz-Marzán, L. M. *Chem. Mater.* **2013**, *25*, 1465−1476.
(49) Wang, Z.; Wen, X.-D.; Hoffmann, R.; Son, J. S.; Li, R.; Fang, C.-C.; Smilgies, D.-M.; Hyeon, T. *Proc. Natl. Acad. Sci. U. S. A.* **2010**, *107*, 17119−17124.

DOI: 10.1021/jacs.5b05629
J. Am. Chem. Soc. 2015, 137, 10297−10303